

Multiple Schottky Barrier-Limited Field-Effect Transistors on a Single Silicon Nanowire with an Intrinsic Doping Gradient

Jorge L. Barreda,[†] Timothy D. Keiper,[†] Mei Zhang,[‡] and Peng Xiong^{*,†}

[†]Department of Physics, Florida State University, Tallahassee, Florida 32306, United States

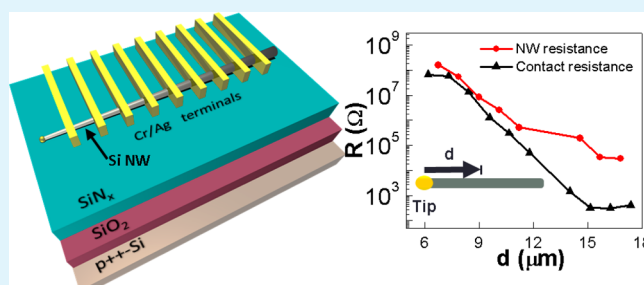
[‡]Department of Industrial and Manufacturing Engineering, College of Engineering, Florida A&M University—Florida State University (FAMU-FSU), Tallahassee, Florida 32310, United States

S Supporting Information

ABSTRACT: In comparison to conventional (channel-limited) field-effect transistors (FETs), Schottky barrier-limited FETs possess some unique characteristics which make them attractive candidates for some electronic and sensing applications. Consequently, modulation of the nano Schottky barrier at a metal–semiconductor interface promises higher performance for chemical and biomolecular sensor applications when compared to conventional FETs with ohmic contacts. However, the fabrication and optimization of devices with a combination of ideal ohmic and Schottky contacts as the source and drain, respectively, present many challenges.

We address this issue by utilizing Si nanowires (NWs) synthesized by a chemical vapor deposition process which yields a pronounced doping gradient along the length of the NWs. Devices with a series of metal contacts on a single Si NW are fabricated in a single lithography and metallization process. The graded doping profile of the NW is manifested in monotonic increases in the channel and junction resistances and variation of the nature of the contacts from ohmic to Schottky of increasing effective barrier height along the NW. Hence multiple single Schottky junction-limited FETs with extreme asymmetry and high reproducibility are obtained on an individual NW. A definitive correlation between increasing Schottky barrier height and enhanced gate modulation is revealed. Having access to systematically varying Schottky barrier contacts on the same NW device provides an ideal platform for identifying optimal device characteristics for sensing and electronic applications.

KEYWORDS: Schottky junction, silicon nanowire, axial inhomogeneous doping, field-effect transistor, asymmetric field-effect transistor, Schottky barrier field-effect transistor



INTRODUCTION

Nanotechnology research has given rise to several potential new paradigms of chemical and biomolecular detection utilizing nanomaterials and mechanical, optical, or electronic responses.^{1–3} A class of nanodevices which has received extensive attention in this regard is nanoscale field-effect transistors (FETs).^{4–6} Such devices have been shown to be capable of label-free sensing of a broad variety of biomolecules including DNA, protein, and virus with high sensitivity and specificity.^{7–9} Perhaps most notably, such devices provide exceptional portability for point-of-care applications. For example, nano-FETs based on individual SnO_2 nanobelts¹⁰ have been studied and adapted for the detection of human cardiac troponin, for potential application of on-site early detection of myocardial ischemia.¹¹

It is generally accepted that the basic sensing mechanism of the nano-FET-based biosensors relies on a change in the electrical conductance of a biofunctionalized FET upon binding of the specific target analyte. However, similar to the electrical gating responses of such devices, the conductance changes in the biosensing could have two distinct origins: the semiconductor channel or the metal–semiconductor interface

(MSI) at the source/drain contacts. This distinction defines two classes of devices: channel-limited and Schottky barrier (SB)-limited sensors. While the focus of the attention in the early stages of the research in nano-FET biosensors was primarily on channel-limited devices,^{10,12–14} in recent years there has been growing interest in the SB-limited sensors which could potentially offer faster and more sensitive detection performance compared with the channel-limited ones.^{12,15–17} This prospect is particularly intriguing thanks to the exponential responses of the SB devices to surface charges, in contrast to the linear responses in channel-limited FETs. However, SB-limited FETs based on nanomaterials such as semiconductor nanowires have not seen extensive studies, primarily because of the difficulties in precise, reproducible control of the metal–semiconductor interface.

For the SB-limited sensors, we can take as a representative example the FETs based on carbon nanotubes (CNTs), which have shown such remarkable properties as high sensitivity and

Received: January 4, 2017

Accepted: March 9, 2017

Published: March 9, 2017

fast response/recovery.^{17–21} The pronounced responses seen in the CNT FETs are believed to be produced mainly by the modulation of the SB contacts formed at the MSI.²² The higher sensitivity and faster response in the SB-limited sensors are attributed to the fact that in the thermionic emission regime the current has an exponential dependence with respect to the SB height (see eqs 2 and 3 below), in contrast to the linear dependence of the modulation of the carrier concentration of the channel utilizing the field effect.^{12,19} Such great tunability of the contact resistance is known not to be exclusive to CNT FETs.^{12,15,23–25} Several groups have demonstrated similar results on a number of materials through comparison of channel-limited and SB-limited sensors under similar conditions.^{12,24} For example, SB FETs have been fabricated based on CNTs and Si NWs and used for hydrogen gas detection,^{19,23} demonstrating that the SB modulation with different channel materials can efficiently detect the same analyte.

For the elucidation of the electron transport and sensing mechanism of the SB-limited devices, it is desirable to have devices with an asymmetric pair of SB source/drain contacts and, if possible, make one of the contacts ohmic. This configuration will ensure that the flow of electrons is limited by one dominant energy barrier, which is modulated by an electric field from a gate electrode or bound analyte molecules. Precise and reproducible modulation of the SB height is desirable but also one of the main challenges for the SB-limited sensors.^{26,27} One common way to obtain devices with significantly asymmetric source/drain contacts is to use metals of different work functions for the two contacts;^{12,26,28} however, this comes with the complication of additional fabrication steps. Another option is to *selectively* anneal one of the contacts to modify its SB height,^{29,30} but this also complicates the fabrication procedure and does not ensure reproducible results. In an alternative approach, axial p–n junctions³¹ and n-type/intrinsic Schottky junctions^{32,33} are produced in individual Si NWs by using a controlled nickel–silicidation process. An elaborate dual-gate structure is further developed to realize multimode (both p-type and n-type) FET operation based on the single Schottky junction in a Si NW.³³

In this work, we report on a new approach for producing single SB-limited FET devices with variable and controllable SB height. The devices are based on individual Si NWs with an axial doping gradient and fabricated with a straightforward process not requiring silicide formation, thereby without any thermal annealing step. The devices result in excellent predictability and reproducibility in the SB contact. The phosphorus-doped silicon NWs are grown via a chemical vapor deposition (CVD) process. The overall phosphorus doping level is controlled by the ratio of the partial pressures of the silane and phosphine precursor gases, while a doping gradient results from distinct dopant incorporation kinetics present in the axial vapor–liquid–solid (VLS) and radial vapor–solid (VS) growth.^{34–36} For each device, a series of Cr/Ag metal contacts are patterned along the length of an individual NW in a single lithography and metallization step. A combination of two-terminal and four-terminal measurements are performed to determine the resistance of each contact and NW section and to clearly decipher the contributions from the SB and the NW channel in the electrical transport measurements. The results reveal a systematic increase of the Si NW channel resistivity and a concurrent exponential increase of the contact resistance along the axial growth direction of the NW from the base (starting point of growth) to the tip (end point

of growth). Using the least resistive contact near the base as the source electrode and one of the other contacts as the drain, we obtain a series of FETs with variable channel and drain contact resistances on the same Si NW. The output characteristics (source-drain I – V) of the devices are measured at different gate voltages and analyzed with a model of a Schottky diode with a series resistance. Such a model device can be described using the thermionic emission theory, which is used to fit the data and extract characteristic parameters.^{37–39} The results clearly demonstrate a systematic enhancement of the gate modulation with increasing predominance by the SB at the drain contact. The device structure thus provides an ideal platform for systematic and quantitative evaluation of the SB-limited FET.

RESULTS AND DISCUSSION

Figure 1a is an SEM image of as-grown Si NWs standing on the substrate, showing high yield and uniformity of a typical growth. A ubiquitous characteristic of the Si NWs is the difference in coloration under bright field for the opposite ends of each NW, being darker (red-like) at the region closer to the base and lighter (yellow-like) on the opposite side (Figure 1b). This is a first indication of a gradual variation of the physical properties of the NWs along the growth direction. In order to explain this change in appearance, the Si NWs can be regarded as cylindrical dielectric cavity antennas.⁴⁰ In this picture, the NWs can trap light and scatter it at specific frequencies when the incident wavelength matches one of the resonance modes. This mechanism has been previously cited to explain the change in color of Si nanostructures⁴¹ and the light interaction properties of other semiconductor nanostructures.^{42–44} In this model, the inelastic light scattering process by the high-index medium (silicon in our case) follows the condition that the wavelength of the trapped light is related to the NW's circumference by an integer number:⁴⁵ $k(\lambda/n) \approx 2\pi r$, where k is an integer, λ is the wavelength of the trapped light, n is the refractive index of the Si NW, and r is the radius of the NW. The change in the Si NW color from red-like (base) to yellow-like (tip) therefore can have two possible origins: the change in the radius of the NW and the change in the refractive index. The latter depends on temperature, doping concentration, and wavelength. Based on previous work,⁴⁶ we surmise that the color change in our Si NWs stems primarily from the radius variation.

Corresponding to the change in color, SEM imaging revealed a gradual increase of the NW diameter from the tip to the base over the entire length of $\sim 25 \mu\text{m}$. Figure 1c shows the SEM images of the base and tip, respectively, of a NW, where a typical change in diameter of about 15% is present. Similar observations were reported for VLS grown NWs when separate precursor gases were used for bulk growth and doping.^{36,47} They were attributed to two distinct mechanisms involved in the growth of such NWs:^{34–36} The first is responsible for the axial growth of the NW via a VLS process, while the second one is a radial growth via a VS process. Other than the small geometric variations, a more important consequence of the dual-growth mode is a significant doping gradient along the axial growth direction. Employing devices with a series of metal electrodes on individual Si NWs, we observed direct manifestations of the doping gradient in systematic variations of both the electrical conductivity of the NWs and the contact resistance and I – V characteristics.

Figure 2 shows the structure of a typical device and the electrical characterization of contact and channel resistances. In

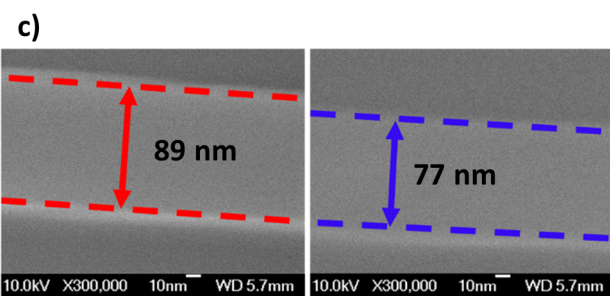
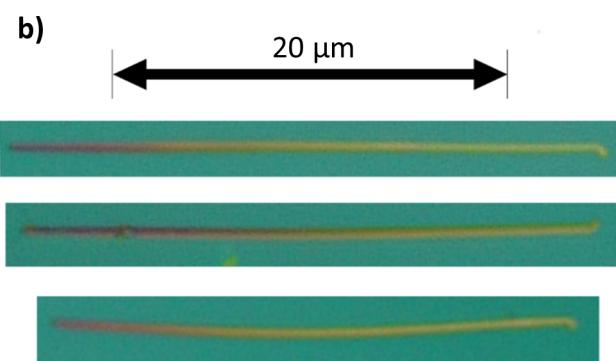
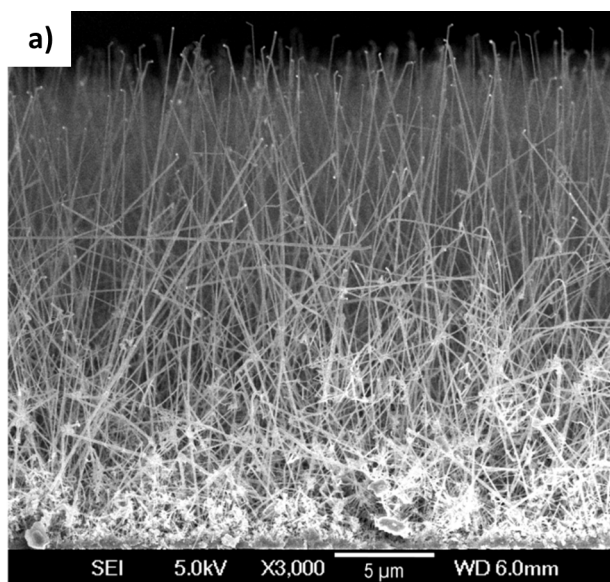


Figure 1. Si NW characteristics. (a) SEM image of the Si NWs grown on the substrate. The kink observed on the tip of the NWs is produced by the change in growth conditions at the end of the process. (b) Distinct change in color under bright field observed along the length of the NWs. The more conductive end is consistently darker (red-like) in comparison to the tip (lighter and yellow-like). (c) Close-up SEM images of a Si NW at its base (left) and tip (right). The base, corresponding to the darker end, has a distinctly larger diameter.

order to determine the resistances of various individual contacts and channels, a series of four-probe and two-probe measurements were carried out with different pin combinations, from which each resistance was calculated (the relevant details are described in the [Supporting Information](#)). Our discussion is focused on a particular device to highlight the main common characteristics; however, more than 30 devices were fabricated showing similar behavior. [Figure 2c](#) displays the values of the zero-bias contact and channel resistance at various distances from the tip of the NW. Immediately notable is that the change

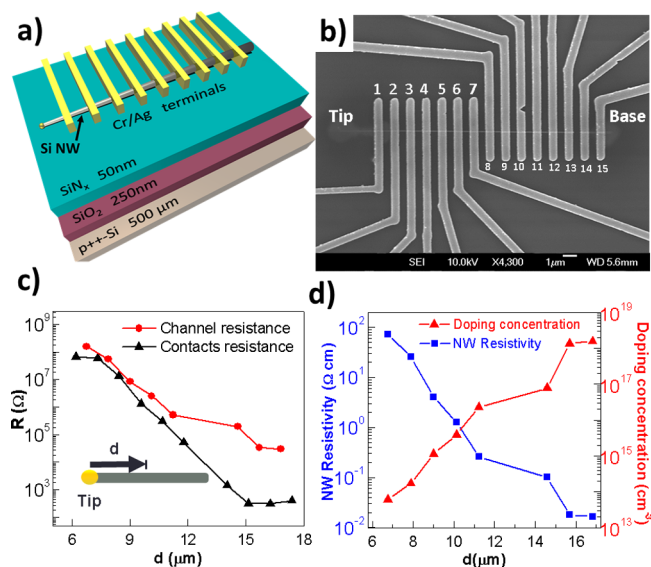


Figure 2. FET device. (a) Schematic diagram and (b) SEM image of an FET device. There are 15 Cr/Ag electrodes equally spaced along the length of a single Si NW. (c) Evolution of the contact and channel (between two consecutive terminals) resistances over $\sim 10 \mu\text{m}$ along the length of the NW. The inset indicates the convention used to measure the distance from the tip of the NW. (d) NW resistivity (blue) along the axial direction calculated from the four-probe measurements. The doping concentration (red) was inferred from the resistivity values in comparison with bulk Si.

in the NW channel resistance is about 4 orders of magnitude over the length of the NW and quasi-exponential, which cannot be attributed to the geometrical changes in the NW cross-section. The variation of the contact resistance is even greater and exhibits an exponential dependence except near the base and the tip where it seems to reach a saturation level. From the four-probe measurements we were able to extract the NW resistivity for the different sections between consecutive terminals. Knowing the resistivity, we estimated the doping concentration via comparison of the resistivity of bulk Si at 300 K.^{48,49} Both resistivity and the deduced doping level are plotted in [Figure 2d](#).

Concomitant with the exponential increases of the channel and junction resistances, the I - V s exhibit increasing non-linearity for junctions located from the base to the tip. Consistent with a gradient in the doping level along the length of the NW, the junctions close to the base exhibit well-defined ohmic behavior; in contrast, the contacts close to the tip show asymmetric nonlinear I - V s typical of a SB. This doping profile and the resulting variation of the I - V characteristics allow us to combine one low-resistance ohmic contact (no. 14 in [Figure 2b](#), the closest contact to the base whose resistance can be accurately determined) with one of a number of SB contacts with increasing barrier height. [Figure 3](#) shows the I - V s and their field-effect modulation for six such combinations, i.e., the output characteristics of the six FETs, on a single Si NW. As shown in [Figure 3a](#), the I - V curves from the least resistive combination, 14–13, are essentially linear and exhibit minimal gate modulation. At the other extreme, the I - V s of combination 14–4 show an asymmetric nonlinear behavior characteristic of a single SB-limited FET. The device also exhibits significantly enhanced gate modulation; it can be turned off at $V_G = -30 \text{ V}$.

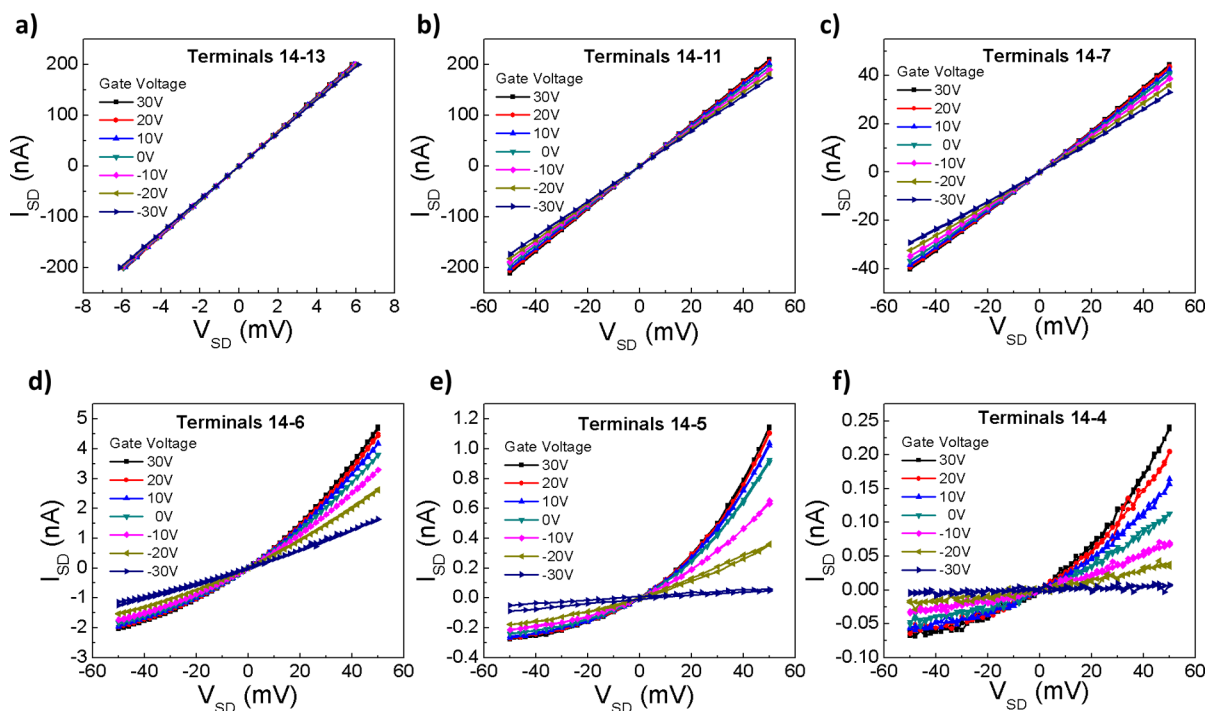


Figure 3. Transport measurements. Two-terminal I - V characteristics for the following combinations: (a) 14-13, (b) 14-11, (c) 14-7, (d) 14-6, (e) 14-5, and (f) 14-4. A systematic increase in the two-terminal resistance is observed, concurrent with increasing nonlinearity of the I - V and the Schottky barrier height closer to the tip of the NW.

For a quantitative understanding of the systematic evolution of the device characteristics observed in Figure 3, we model each FET with substantial asymmetry in the I - V as a Schottky junction (drain) in series with a resistor (channel),³⁷⁻³⁹ as represented in the inset of Figure 4b. In this model, the applied voltage V , the Schottky diode voltage V_{sh} , the series resistance R_s , and the current I are related as

$$V = V_{sh} + IR_s \quad (1)$$

This helps isolate the contribution of the Schottky junction to the transport, which can then be analyzed by fitting the I - V to the thermionic emission theory, with the saturation current I_0 , ideality factor n , and the series resistance R_s as the adjustable parameters. The measured I - V s are fit to

$$I = I_0 \left[\exp\left(\frac{e(V - IR_s)}{nk_B T}\right) - 1 \right] \quad (2)$$

where e is the electron charge, k_B is the Boltzmann constant, T is the absolute temperature, V is the voltage across the source-drain terminals in the device, and from the expression for the saturation current I_0 :

$$I_0 = SA^* T^2 \exp\left(-\frac{e\phi_{\text{barrier}}}{k_B T}\right) \quad (3)$$

we can extract the effective Schottky barrier height ϕ_{barrier} where S is the junction area and A^* is the modified Richardson's constant (for n-Si, $A^* \approx 120 \text{ A cm}^{-2} \text{ K}^{-2}$).⁵⁰

Based on eq 2, we utilized a nonlinear least-squares Marquardt-Levenberg fitting algorithm to extract the parameters R_s , n , and I_0 .⁵¹ Once the best value of the parameter I_0 is obtained, the effective SB height can be calculated as

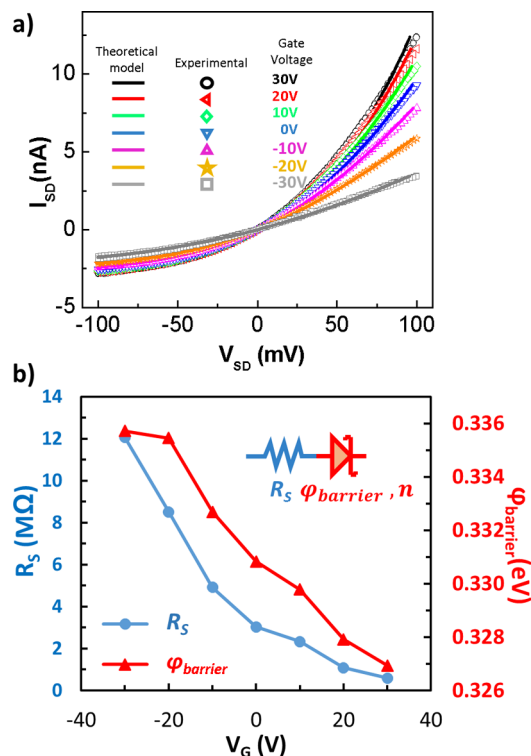


Figure 4. Thermionic emission model fitting of the I - V . (a) Experimental data (open figures) of two-terminal I - V s and thermionic emission model fitting (solid lines) for terminal combination 14-6. The different colors/figures represent different gate voltages. (b) Series resistance (blue circles) and the effective SB height (red triangles) obtained from the fittings for different gate voltages. The inset shows a schematic diagram of the theoretical model with the corresponding fitting parameters.

$$\varphi_{\text{barrier}} = \frac{k_{\text{B}}T}{e} \log\left(\frac{SA^*T^2}{I_0}\right) \quad (4)$$

In Figure 4a, we show a typical set of fitting results (solid lines) for the experimental I - V curves (open figures) at different gate voltages for the same FET (14–6). Figure 4b shows the changes of the resulting SB height (red triangles) and the series resistance (blue circles) with respect to the gate voltage. The series resistance decreases roughly exponentially with increasing gate voltage. This behavior is typical of n-type semiconductors²⁸ and is most likely due to the gate tuning of the phosphorus-doped Si NW channel. In order to validate this hypothesis, we compare the series resistances obtained from the fitting of the two-probe I - V s with the channel resistance determined from the four-probe measurements, the results are shown in Figure 5a. To facilitate a more accurate comparison

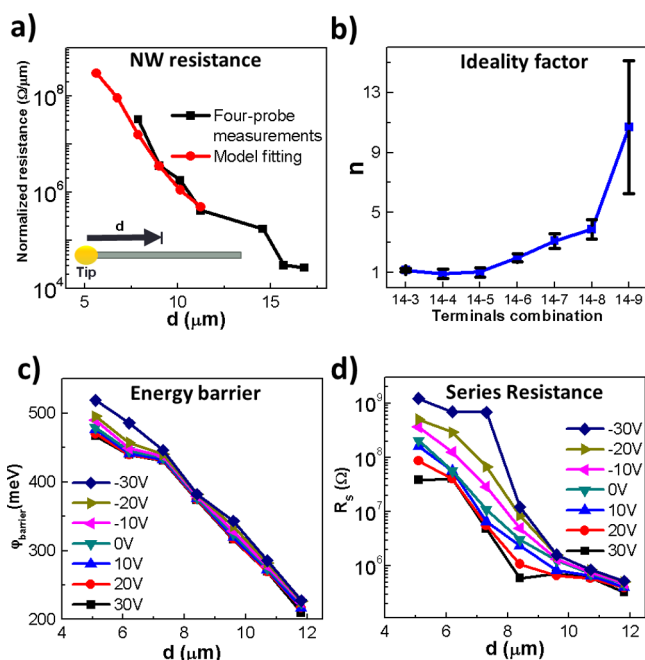


Figure 5. Fitting results. (a) Series resistance extracted from the fitting of the two-terminal I - V s (red) and the NW resistance obtained from the four-probe measurements (black). The overlap of the two curves supports the applicability of the thermionic emission model for the I - V analysis. (b) Ideality factor extracted from the I - V fittings. The values are 1 for the three drain terminals closest to the tip of the NW, indicating they are ideal Schottky junctions. (c) Effective SB height and (d) series resistance determined from the I - V fittings for different gate voltages. Toward the tip of the NW, the SB height increases linearly while the series resistance increases approximately exponentially.

between the two, we normalize both resistance values to the channel length for each FET (terminal combination). For the resistance values obtained from the four-probe measurements, we use the center-to-center separation between the voltage terminals as the channel length; for the series resistance values obtained from the fitting of the two-terminal FET (source-drain) I - V , we take the length of the channel as the distance between the inner edges of the terminals. It is evident that in the region where both types of measurements were performed, the resistances determined from the two methods are essentially the same, providing strong evidence in support of

the validity of the model employed for the I - V analysis. It is worth noting that the four-probe measurement can be performed all the way to the base of the NW (the most conductive section) where the I - V s are essentially linear and the SB model (thermionic emission) fitting is not applicable; on the other hand, the two-terminal I - V measurement and its modified SB model fitting can be extended into the most resistive side near the tip. Therefore, the two types of measurements are complementary in producing the channel resistance profile over the broadest length along the NW. Figure 5b shows the variation of the ideality factor of the SB for different drain terminals; the error bars were taken as the standard deviation between the values obtained at different gate voltages. Panels c and d of Figure 5 present the effective SB height and the series resistance respectively at different gate voltages for different positions along the length of the Si NW.

CONCLUSIONS

The detailed discussion of the results will be based on the data from the device described above. However, we emphasize that more than 30 samples have been fabricated and measured; similar characteristics were observed in all of them, showing excellent reproducibility. The outstanding reproducibility is a distinct quality of these NW devices, which provides a rather straightforward pathway to obtaining single SB-limited FETs of predictable performance.

Analyzing the evolution of the NW resistivity, it is possible to deduce an effective doping level evolving along the channel if we compare such values with those of bulk Si (Figure 2d). Other groups have reported an inhomogeneous doping level in similar NWs.^{34,47} The doping concentration that we obtained can be taken as a radial average, knowing that the dopants likely have a radially increasing gradient due to the incorporation of the P atoms in the VS process. The calculated radial average concentration changes 4 orders of magnitude from 10^{14} to 10^{18} cm^{-3} over approximately 10 μm of the NW. The close relation between the change in doping concentration and the observed exponential variation along the NW length facilitates the high degree of control in fabricating these FETs with extreme behavior.

Summarized in Figures 3, 4, and 5, we observe an unambiguous increase in the effective SB height for a series of Schottky junctions located along a Si NW. For the presented device, the SB height ranges from ~ 0.210 to ~ 0.520 eV. The emergence and gradual increase in the SB is responsible for the evolution of the junction I - V characteristics from linear to rectifying behavior and the corresponding exponential increase in contact resistance as observed through the I - V s of Figure 3a–f. Examining more closely the ideality factor parameters in Figure 5b, the three contacts closest to the tip of the NW have an ideality factor of 1 within the standard deviation, indicating that they behave as ideal Schottky junctions and the thermionic emission model is valid. Moving further away from the tip, the ideality factor increases until it is no longer possible to reliably fit the experimental data to the theoretical model.

The exponential changes in contact and channel resistance in the axial direction of the Si NWs support the model of two distinct doping mechanisms related with the VLS and the VS growths. The high yield and consistency in the characteristics observed in our more than 30 measured Si NWs promise the capability of excellent control for devices where it is desirable to have asymmetrical contacts. We demonstrated that devices with a single SB contact can be fabricated with our Si NW with no

need of any thermal annealing and with a single metallization process where an ideal Schottky junction can be readily achieved. The ability to reliably and reproducibly produce SB-limited FETs affords the opportunity to apply such devices for sensing experiments where a systematic comparison and tuning can be realized. The gain in the gating performance, taking one ohmic and one SB contact, is a primary feature for the application in sensor devices. Here we have shown gate modulation over orders of magnitude utilizing single SB FETs over a range of barrier heights. The gating performance would be improved by decreasing the dielectric thickness, choosing a better dielectric, or conducting experiments with an ionic liquid gate or in an extended gate scheme. We expect the detailed characterization and understanding presented in this work will be useful to furthering the development of efficient sensing devices.

EXPERIMENTAL PROCEDURES

Nanowire Synthesis. The phosphorus-doped Si NWs were synthesized by CVD via VLS and VS methods. Previously, we have reported the formation of Si NWs on different substrates with similar growth conditions.⁵² For the Si NWs utilized in this particular study, the growths took place on Si substrates coated with 4 nm of gold. The gold films were deposited via thermal evaporation with vacuum levels on the order of 10^{-6} Torr and deposition rates of $\sim 1 \text{ \AA s}^{-1}$. The gold films are granular, and the gold grains act as catalyst particles for the formation of the Si NWs. The coated substrates were loaded into the CVD system. The system was evacuated and then filled with H_2 to reach a pressure of 20 Torr. Silane (SiH_4) was used as the precursor gas, and the growth occurred at $460 \text{ }^\circ\text{C}$ for a period of 15 min at a flow rate of $80 \text{ cm}^3(\text{STP}) \text{ min}^{-1}$. For the P-doping of the NWs, phosphine (PH_3) gas was added to the growth environment and the doping level was controlled by its flow rate. At the end of the process, the reaction gas flow was turned off and the furnace was cooled to room temperature before venting. Si NWs were obtained from four different growths with phosphine flow rates of 5, 10, 11, and $12 \text{ cm}^3(\text{STP}) \text{ min}^{-1}$, under otherwise identical conditions. The Si NWs were removed from the substrates and dispersed in isopropanol via sonication for later use.

Preparation of Device. The devices were fabricated via a standard nanolithographic and metallization process. The Si NWs in the isopropanol solution are dispersed onto a p++-Si/ SiO_2 / SiN_x substrate, as indicated in the schematic diagram of Figure 2a. One Si NW was identified by optical microscopy for further processing. The SiN_x and SiO_2 layers, with a thickness of 50 and 250 nm, respectively, are used as the gating dielectric, and the degenerately doped Si layer for back-gating. A pattern of 15 electrodes is defined using electron-beam lithography on the same NW. After development of the pattern, the sample was dipped in buffered hydrofluoric acid (Transene BUFFER-HF Improved) for 8 s to remove the native oxide layer on the NW. The sample was placed in high vacuum immediately following the etching, where Cr (20 nm) and then Ag (200 nm) were deposited by thermal evaporation with vacuum levels on the order of 10^{-6} Torr and deposition rates of $\sim 1 \text{ \AA s}^{-1}$. The final device was obtained after a gentle lift-off process (avoiding ultrasonication) in acetone. Figure 2b shows an SEM image of a finished device; the electrodes have a width of $0.61 \pm 0.01 \text{ }\mu\text{m}$ with a separation of $0.51 \pm 0.02 \text{ }\mu\text{m}$, values typical of the devices measured. The samples were measured under vacuum to avoid variations due to ambient humidity. The device structure enables simultaneous four-probe and two-probe electrical resistance measurements, which yield the resistances of each NW section and contact along the length of the NW from the base to the tip.

Electrical Transport Measurements. Once the devices were ready they were put under vacuum to perform the measurements. A source/meter Keithley 2400 was used to take the two-probe and four-probe measurements at room temperature. For the two-probe measurements, the voltage was applied and the current was measured in the same terminals. For the four-probe measurements, the current

was applied in the two external terminals and the voltage was measured in the internal ones. The external terminals were the closest ones to the internal terminals.

ASSOCIATED CONTENT

Supporting Information

The Supporting Information is available free of charge on the ACS Publications website at DOI: 10.1021/acsami.7b00144.

Calculation of contact and channel resistances (PDF)

AUTHOR INFORMATION

Corresponding Author

*E-mail: xiong@physics.fsu.edu.

ORCID

Jorge L. Barreda: 0000-0001-9816-9389

Notes

The authors declare no competing financial interest.

ACKNOWLEDGMENTS

We acknowledge funding support from NSF Grant DMR-1308613.

ABBREVIATIONS

CNTs, carbon nanotubes
CVD, chemical vapor deposition
FET, field-effect transistor
MSI, metal–semiconductor interface
NW, nanowire
SB, Schottky-energy barrier
VLS, vapor–liquid–solid
VS, vapor–solid

REFERENCES

- (1) Kelley, S. O.; Mirkin, C. A.; Walt, D. R.; Ismagilov, R. F.; Toner, M.; Sargent, E. H. Advancing the Speed, Sensitivity and Accuracy of Biomolecular Detection Using Multi-Length-Scale Engineering. *Nat. Nanotechnol.* **2014**, *9* (12), 969–980.
- (2) Erickson, D.; Mandal, S.; Yang, A. H. J.; Cordovez, B. Nanobiosensors: Optofluidic, Electrical and Mechanical Approaches to Biomolecular Detection at the Nanoscale. *Microfluid. Nanofluid.* **2008**, *4* (1–2), 33–52.
- (3) Turner, A. P. F. Biosensors: Sense and Sensibility. *Chem. Soc. Rev.* **2013**, *42* (8), 3184–3196.
- (4) Huang, H. T.; Liang, B.; Liu, Z.; Wang, X. F.; Chen, D.; Shen, G. Z. Metal Oxide Nanowire Transistors. *J. Mater. Chem.* **2012**, *22* (27), 13428–13445.
- (5) Liu, S.; Guo, X. Carbon Nanomaterials Field-Effect-Transistor-Based Biosensors. *NPG Asia Mater.* **2012**, *4*, e23.
- (6) Noor, M. O.; Krull, U. J. Silicon Nanowires as Field-Effect Transducers for Biosensor Development: A Review. *Anal. Chim. Acta* **2014**, *825*, 1–25.
- (7) Zheng, G.; Patolsky, F.; Lieber, C. M. Multiplexed Electrical Detection of Single Viruses. *MRS Online Proc. Libr.* **2004**, *828*, 79–84.
- (8) Patolsky, F.; Zheng, G. F.; Hayden, O.; Lakadamyali, M.; Zhuang, X. W.; Lieber, C. M. Electrical Detection of Single Viruses. *Proc. Natl. Acad. Sci. U. S. A.* **2004**, *101* (39), 14017–14022.
- (9) Sorgenfrei, S.; Chiu, C. Y.; Gonzalez, R. L., Jr.; Yu, Y.-J.; Kim, P.; Nuckolls, C.; Shepard, K. L. Label-Free Single-Molecule Detection of DNA-Hybridization Kinetics with a Carbon Nanotube Field-Effect Transistor. *Nat. Nanotechnol.* **2011**, *6* (2), 126–132.
- (10) Cheng, Y.; Xiong, P.; Fields, L.; Zheng, J. P.; Yang, R. S.; Wang, Z. L. Intrinsic Characteristics of Semiconducting Oxide Nanobelt Field-Effect Transistors. *Appl. Phys. Lett.* **2006**, *89* (9), 093114.

- (11) Cheng, Y.; Chen, K. S.; Meyer, N. L.; Yuan, J.; Hirst, L. S.; Chase, P. B.; Xiong, P. Functionalized SnO₂ Nanobelt Field-Effect Transistor Sensors for Label-Free Detection of Cardiac Troponin. *Biosens. Bioelectron.* **2011**, *26* (11), 4538–4544.
- (12) Hu, Y. F.; Zhou, J.; Yeh, P. H.; Li, Z.; Wei, T. Y.; Wang, Z. L. Supersensitive, Fast-Response Nanowire Sensors by Using Schottky Contacts. *Adv. Mater.* **2010**, *22* (30), 3327–3332.
- (13) Stern, E.; Wagner, R.; Sigworth, F. J.; Breaker, R.; Fahmy, T. M.; Reed, M. A. Importance of the Debye Screening Length on Nanowire Field Effect Transistor Sensors. *Nano Lett.* **2007**, *7* (11), 3405–3409.
- (14) Cui, Y.; Zhong, Z. H.; Wang, D. L.; Wang, W. U.; Lieber, C. M. High Performance Silicon Nanowire Field Effect Transistors. *Nano Lett.* **2003**, *3* (2), 149–152.
- (15) Zorgiebel, F.; Pregl, S.; Romhildt, L.; Opitz, J.; Weber, W.; Mikolajick, T.; Baraban, L.; Cuniberti, G. Schottky Barrier-Based Silicon Nanowire pH Sensor with Live Sensitivity Control. *Nano Res.* **2014**, *7* (2), 263–271.
- (16) Yang, Z.; Dou, X. C.; Zhang, S. L.; Guo, L. J.; Zu, B. Y.; Wu, Z. F.; Zeng, H. B. A High-Performance Nitro-Explosives Schottky Sensor Boosted by Interface Modulation. *Adv. Funct. Mater.* **2015**, *25* (26), 4039–4048.
- (17) Suehiro, J.; Imakiire, H.; Hidaka, S.; Ding, W. D.; Zhou, G. B.; Imasaka, K.; Hara, M. Schottky-Type Response of Carbon Nanotube NO₂ Gas Sensor Fabricated onto Aluminum Electrodes by Dielectrophoresis. *Sens. Actuators, B* **2006**, *114* (2), 943–949.
- (18) Byon, H. R.; Choi, H. C. Network Single-Walled Carbon Nanotube-Field Effect Transistors (SWNT-FETs) with Increased Schottky Contact Area for Highly Sensitive Biosensor Applications. *J. Am. Chem. Soc.* **2006**, *128* (7), 2188–2189.
- (19) Zhang, M. L.; Brooks, L. L.; Chartuprayoon, N.; Bosze, W.; Choa, Y. H.; Myung, N. V. Palladium/Single-Walled Carbon Nanotube Back-to-Back Schottky Contact-Based Hydrogen Sensors and Their Sensing Mechanism. *ACS Appl. Mater. Interfaces* **2014**, *6* (1), 319–326.
- (20) Qi, P.; Vermesh, O.; Grecu, M.; Javey, A.; Wang, O.; Dai, H.; Peng, S.; Cho, K. J. Toward Large Arrays of Multiplex Functionalized Carbon Nanotube Sensors for Highly Sensitive and Selective Molecular Detection. *Nano Lett.* **2003**, *3* (3), 347–351.
- (21) Cantalini, C.; Valentini, L.; Armentano, I.; Lozzi, L.; Kenny, J. M.; Santucci, S. Sensitivity to NO₂ and Cross-Sensitivity Analysis to NH₃, Ethanol and Humidity of Carbon Nanotubes Thin Film Prepared by PECVD. *Sens. Actuators, B* **2003**, *95* (1–3), 195–202.
- (22) Chen, R. J.; Choi, H. C.; Bangsaruntip, S.; Yenilmez, E.; Tang, X. W.; Wang, Q.; Chang, Y. L.; Dai, H. J. An Investigation of the Mechanisms of Electronic Sensing of Protein Adsorption on Carbon Nanotube Devices. *J. Am. Chem. Soc.* **2004**, *126* (5), 1563–1568.
- (23) Skucha, K.; Fan, Z. Y.; Jeon, K.; Javey, A.; Boser, B. Palladium/Silicon Nanowire Schottky Barrier-Based Hydrogen Sensors. *Sens. Actuators, B* **2010**, *145* (1), 232–238.
- (24) Singh, N.; Yan, C. Y.; Lee, P. S.; Comini, E. Sensing Properties of Different Classes of Gases Based on the Nanowire-Electrode Junction Barrier Modulation. *Nanoscale* **2011**, *3* (4), 1760–1765.
- (25) Javey, A.; Guo, J.; Wang, Q.; Lundstrom, M.; Dai, H. J. Ballistic Carbon Nanotube Field-Effect Transistors. *Nature* **2003**, *424* (6949), 654–657.
- (26) Larson, J. M.; Snyder, J. P. Overview and Status of Metal S/D Schottky-Barrier MOSFET Technology. *IEEE Trans. Electron Devices* **2006**, *53* (5), 1048–1058.
- (27) Koo, S. M.; Edelstein, M. D.; Li, Q. L.; Richter, C. A.; Vogel, E. M. Silicon Nanowires as Enhancement-Mode Schottky Barrier Field-Effect Transistors. *Nanotechnology* **2005**, *16* (9), 1482–1485.
- (28) Sze, S. M.; Kwok, K. Ng. *Physics of Semiconductor Devices*, 3 ed.; John Wiley & Sons, 2006.
- (29) Brillson, L. J.; Mosbacker, H. L.; Hetzer, M. J.; Strzhemechny, Y.; Look, D. C.; Cantwell, G.; Zhang, J.; Song, J. J. Surface and near-Surface Passivation, Chemical Reaction, and Schottky Barrier Formation at ZnO Surfaces and Interfaces. *Appl. Surf. Sci.* **2008**, *254* (24), 8000–8004.
- (30) Byon, K.; Tham, D.; Fischer, J. E.; Johnson, A. T. Systematic Study of Contact Annealing: Ambipolar Silicon Nanowire Transistor with Improved Performance. *Appl. Phys. Lett.* **2007**, *90* (14), 143513.
- (31) Hoffmann, S.; Bauer, J.; Ronning, C.; Stelzner, T.; Michler, J.; Ballif, C.; Sivakov, V.; Christiansen, S. H. Axial p-n Junctions Realized in Silicon Nanowires by Ion Implantation. *Nano Lett.* **2009**, *9* (4), 1341–1344.
- (32) Weber, W. M.; Geelhaar, L.; Graham, A. P.; Unger, E.; Duesberg, G. S.; Liebau, M.; Pamler, W.; Cheze, C.; Riechert, H.; Lugli, P.; Kreupl, F. Silicon-Nanowire Transistors with Intruded Nickel-Silicide Contacts. *Nano Lett.* **2006**, *6* (12), 2660–2666.
- (33) Glassner, S.; Zeiner, C.; Periwal, P.; Baron, T.; Bertagnolli, E.; Lugstein, A. Multimode Silicon Nanowire Transistors. *Nano Lett.* **2014**, *14* (11), 6699–6703.
- (34) Perea, D. E.; Hemesath, E. R.; Schwalbach, E. J.; Lensch-Falk, J. L.; Voorhees, P. W.; Lauhon, L. J. Direct Measurement of Dopant Distribution in an Individual Vapour-Liquid-Solid Nanowire. *Nat. Nanotechnol.* **2009**, *4* (5), 315–319.
- (35) Koren, E.; Berkovitch, N.; Rosenwaks, Y. Measurement of Active Dopant Distribution and Diffusion in Individual Silicon Nanowires. *Nano Lett.* **2010**, *10* (4), 1163–1167.
- (36) Connell, J. G.; Yoon, K.; Perea, D. E.; Schwalbach, E. J.; Voorhees, P. W.; Lauhon, L. J. Identification of an Intrinsic Source of Doping Inhomogeneity in Vapor-Liquid-Solid-Grown Nanowires. *Nano Lett.* **2013**, *13* (1), 199–206.
- (37) Tung, R. T. Recent Advances in Schottky Barrier Concepts. *Mater. Sci. Eng., R* **2001**, *35* (1–3), 1–138.
- (38) Rodrigues, A. M. Extraction of Schottky Diode Parameters from Current-Voltage Data for a Chemical-Vapor-Deposited Diamond/Silicon Structure over a Wide Temperature Range. *J. Appl. Phys.* **2008**, *103* (8), 083708.
- (39) Ahmed, K.; Chiang, T. Schottky Barrier Height Extraction from Forward Current-Voltage Characteristics of Non-Ideal Diodes with High Series Resistance. *Appl. Phys. Lett.* **2013**, *102* (4), 042110.
- (40) Long, S. A.; McCallister, M. W.; Shen, L. C. The Resonant Cylindrical Dielectric Cavity Antenna. *IRE Trans. Antennas Propag.* **1983**, *31* (3), 406–412.
- (41) Cao, L. Y.; Fan, P. Y.; Barnard, E. S.; Brown, A. M.; Brongersma, M. L. Tuning the Color of Silicon Nanostructures. *Nano Lett.* **2010**, *10* (7), 2649–2654.
- (42) Cao, L. Y.; Nabet, B.; Spanier, J. E. Enhanced Raman Scattering from Individual Semiconductor Nanocones and Nanowires. *Phys. Rev. Lett.* **2006**, *96* (15), 157402.
- (43) Muskens, O. L.; Diedenhofen, S. L.; Kaas, B. C.; Algra, R. E.; Bakkers, E. P. A. M.; Gómez Rivas, J.; Lagendijk, A. Large Photonic Strength of Highly Tunable Resonant Nanowire Materials. *Nano Lett.* **2009**, *9* (3), 930–934.
- (44) Cao, L. Y.; Park, J. S.; Fan, P. Y.; Clemens, B.; Brongersma, M. L. Resonant Germanium Nanoantenna Photodetectors. *Nano Lett.* **2010**, *10* (4), 1229–1233.
- (45) Cao, L. Y.; White, J. S.; Park, J. S.; Schuller, J. A.; Clemens, B. M.; Brongersma, M. L. Engineering Light Absorption in Semiconductor Nanowire Devices. *Nat. Mater.* **2009**, *8* (8), 643–647.
- (46) Zhou, Z. H.; Choi, B.; Flik, M.; Fan, S.; Reif, R. Epifilm Thickness Measurements Using Fourier Transform Infrared Spectroscopy: Effect of Refractive Index Dispersion and Refractive Index Measurement. *J. Appl. Phys.* **1994**, *76* (4), 2448–2454.
- (47) Schlitz, R. A.; Perea, D. E.; Lensch-Falk, J. L.; Hemesath, E. R.; Lauhon, L. J. Correlating Dopant Distributions and Electrical Properties of Boron-Doped Silicon Nanowires. *Appl. Phys. Lett.* **2009**, *95* (16), 162101.
- (48) Thurber, W. R.; Mattis, R. L.; Liu, Y. M.; Filliben, J. J. Resistivity-Dopant Density Relationship for Phosphorus-Doped Silicon. *J. Electrochem. Soc.* **1980**, *127* (8), 1807–1812.
- (49) Thurber, W. R.; Mattis, R. L.; Liu, Y. M.; Filliben, J. J. *The Relationship between Resistivity and Dopant Density for Phosphorus- and Boron-Doped Silicon*, NBS Special Publication 400-64; U.S. Government Printing Office: Washington, DC, USA, 1981.

(50) Andrews, J. M.; Lepselter, M. P. Reverse Current-Voltage Characteristics of Metal-Silicide Schottky Diodes. *Solid-State Electron.* **1970**, *13* (7), 1011–1023.

(51) Hauser, J. R. *Numerical Methods for Nonlinear Engineering Models*. Springer, 2009.

(52) Liu, T.; Liang, R.; Okoli, O.; Zhang, M. Fabrication of Silicon Nanowire on Freestanding Multiwalled Carbon Nanotubes by Chemical Vapor Deposition. *Mater. Lett.* **2015**, *159*, 353–356.